J. At. Mol. Sci.
doi: 10.4208/jmas.063012.072912a

Vol. **4** , No. 3 , pp. 225-234
August 2013

Insight into interaction mechanism of the inhibitor pDI6W with MDM2 based on molecular dynamics

Jian-Zhong Chen[a,*], Zhi-Qiang Liang[a], Qing-Gang Zhang[b], Xiao-Yang Liu[c], Wei Wang[a], and Jin-Qing Liu[a]

[a] *School of Science, Shandong Jiaotong University, Jinan 250023, China*
[b] *College of Physics and Electronics, Shandong Normal University, Jinan 250014, China*
[c] *Department of Electronics and Engineering, Jinan Vocational college, Jinan 250014, China*

Received 30 June 2012; Accepted (in revised version) 29 July 2012
Published Online 28 June 2013

Abstract. The p53-MDM2 interaction has been an important target of drug design curing cancers. In this work, Molecular dynamics (MD) simulation coupled with molecular mechanics/Poisson Boltzmann surface area method (MM-PBSA) is performed to calculate binding free energy of peptide inhibitor pDI6W to MDM2. The results show that van der Waals energy is the dominant factor of the pDI6W-MDM2 interaction. Cross-correlation matrix calculated suggests that the main motion of the residues in MMDM2 induced by the inhibitor binding is anti-correlation motion. The calculations of residue-residue interactions between pDI6W and MDM2 not only prove that five residues Phe19′, Trp22′, Trp23′, Leu26′ and Thr27′ from pDI6W can produce strong interactions with MDM2, but also show that CH-π, CH-CH and $\pi-\pi$ interactions drive the binding of pDI6W in the hydrophobic cleft of MDM2. This study can provide theoretical helps for anti-cancer drug designs.

PACS: 87.15._v; 87.64.Dz

Key words: molecular dynamics simulation, cross-correlation matrix, p53-MDM2 interaction, binding free energy, MM-PBSA

1 Introduction

Currently, the tumor suppressor protein is a protein studied extensively, and it plays an important role in the regulation of the cell cycle and DNA repair[1]. The active p53 can well suppress oncogenesis and effectively protect host cell from cancer[2]. MDM2 can

*Corresponding author. *Email address:* chenjianzhong1970@163.com (J. Z. Chen)

bind directly to p53 and inhibit the activity of p53. In fact, the overexpression of MDM2 occurs in almost 50% of cancers in the world[3, 4]. Thus, the inhibition of the p53-MDM2 interaction becomes a new approach for cancer therapy.

In order to disturb the binding of MDM2 to p53, a few groups have imitate the interactions of three residues Phe19, Trp23 and Leu26 from p53 with MDM2 to design some inhibitors with high affinity[5-7]. The inhibitor pDI6W designed by Phan J *et al.* can bind to MDM2 with binding constant Ki of 36 nmol[8]. Thus, insights into the molecular basis of the pDI6W-MDM2 interaction are helpful for the designs of anti-cancer drugs.

Recently, molecular dynamics (MD) simulation and molecular mechanics/poisson Boltzmann surface area method (MM-PBSA) have been successfully used to study the protein-protein interactions [9-18]. These two methods can efficiently understand the conformation changes of proteins induced by the inhibitor binding and explore the structure-function relation of proteins. At the same time, MD simulation can also provide important dynamic information for the rational designs of small molecule inhibitors.

In this work, the crystal structure (ID: 3JZR) from protein data bank (PDB) is used as the initial model for MD simulation[8], and Fig. 1 depicts the structure of the pDI6W-MDM2 complex. Cross-correlation matrix is computed to investigate the conformation changes of MDM2 induced by the inhibitor binding. The residue-based free energy decomposition is performed to calculate the residue-residue interaction. The results prove that the CH-π, CH-CH and $\pi-\pi$ interactions drive the binding of the inhibitor pDI6W in the hydrophobic cleft of MDM2.

2 Theory and method

2.1 MD simulation

The crystal structure (ID: 3JZR) taken from PDB is used for the starting structure for MD simulation. All crystal water molecules are kept in the starting model. All missing

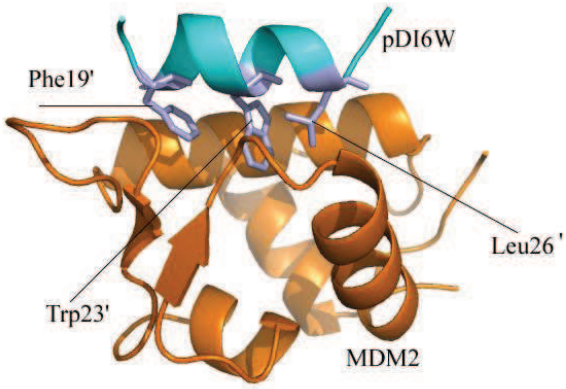

Figure 1: Structure of the pDI6W-MDM2 complex. MDM2 and pDI6W are showed in orange and cyan, respectively, the residues Phe19', Trp23' and Leu26' are displayed in stick mode.

hydrogen atoms are added by using the leap module in Amber 12[19]. The force field parameters of MDM2, pDI6W and water molecule are produced by using the force field ff99SB. The pDI6W-MDM2 complex is solvated in an octahedral periodic box of TIP3P water molecules, and the distance between the edges of the water box and the closet atom of solutes is at least 10 Å. Two chloride ions are placed around the complex to neutralize the charges of the system.

MD simulation is performed by using the sander module in Amber 12. To remove some bad contacts between the complex and the solvent molecules, the system is subject to energy minimization in two stages. Firstly, the solvent molecules and counterions are minimized by freezing the solute using a harmonic constraint of a strength of 100 kcal·mol^{-1}·Å^{-2}. Secondly, the entire system is minimized without restriction. Each stage is carried out using the steepest descent minimization of 1000 steps followed by a conjugate gradient minimization of 3000 steps. Then, the system is heated from 0 to 300 K in 100 ps and equilibrated at 300 K for another 100 ps. Finally, 10 ns MD simulation without restriction is run at 1 atm and 300 K. During the simulation, the SHAKE method is used to constraint the covalent bonds involving hydrogen atom[20]. The time step is set as 2 fs. The particle mesh Ewald (PME) method is applied to compute the long-range electrostatic interactions. The cutoff distances for the long-range electrostatic and van der Waals interaction are set to 10 Å. To avoid the edge effects, the periodic boundary condition is adopted. At the same time, the energies of the system and the root-mean-squared deviation (RMSD) of the backbone atoms relative to the initial minimized structure are monitored to evaluate the reliability of dynamics equilibrium.

2.2 Calculations of binding free energy by using MM-PBSA method

A total number of 100 snapshots are taken from the last 2 ns of the MD trajectory with an interval 10 ps. The MM-PB/SA method and nmod module, which is implemented in Amber12, are applied to compute the binding free energy of pDI6W to MDM2. In this approach, the binding free energy (ΔG) are approximated by

$$\Delta G = \Delta E_{gas} + \Delta G_{sol} - T\Delta S \tag{1}$$

Where ΔE_{gas} is standard molecular mechanical energy in gas phase, $\Delta G - sol$ is the solvation free energy, and $T\Delta S$ is a term involving the entropy effect. The molecular mechanical energy (ΔE_{gas}) can further be expressed as

$$\Delta E_{gam} = \Delta E_{int} + \Delta E_{vdw} + \Delta E_{ele} \tag{2}$$

where ΔE_{int}, ΔE_{vdw} and ΔE_{ele} represent the internal energy contribution from bonds, angles and torsions, the van der Waals and electrostatic interactions in gas phase, respectively. The solvation free energy (ΔG_{sol}) is further divided into two components:

$$\Delta G_{sol} = \Delta G_{pb} + \Delta G_{surf} \tag{3}$$

where ΔG_{pb} and ΔG_{surf} are polar and non-polar contributions to the solvation free energy, respectively. The former component is computed using the pbsa program. The dielectric constant inside the solute is set to 1.0 and 80.0 in the solvent in our calculations. Whereas the latter term is determined by

$$\Delta G_{surf} = \gamma SASA + \beta \tag{4}$$

where SASA is the solvent-accessible surface area and was calculated with the MSMS program. In this work, the values for γ and β was set to 0.00542 kcal·mol^{-1}·Å^{-2} and 0.92 kcal·mol^{-1}, respectively. $T\Delta S$ is the contributions of the conformational entropies to binding free energy. This term is calculated by using the normal-mode analysis and classical thermodynamics.

2.3 Cross-correlation analysis

To investigate the extent of correlation motions due to the formation of the pDI6W-MDM2 complexes, the cross-correlation matrix, C_{ij}, which reflects the fluctuations of coordinates of the C_α atoms relative to its average positions from the last 2 ns of the simulations, is determined by the following equation

$$C(i,j) = <\Delta r_i \times \Delta r_i> / (<\Delta r_j^2><\Delta r_j^2>)^{1/2} \tag{5}$$

where angle bracket represents an average over sampled period and indicates the deviation of the C_α atom of the ith residue from its mean position. The value of the C_{ij} fluctuates in the range from -1 to 1. Positive C_{ij} represents a correlated motion between the ith residue and the jth residue, while negative C_{ij} describes an anticorrelated motion.

3 Results and discussion

3.1 Stability of dynamics equilibrium

To evaluate the reliable stability of the MD trajectory, the RMSD value of the MDM2 backbone atoms relative to the initial minimized structure through the simulation phase is calculated by using the ptraj module of Amber 12 (shown in Fig. 2). According to Fig. 2, one can see that the complex has reached the equilibrium about after 4.5 ns of the simulation phase. The average RMSD value of MDM2 is 1.41 Å and the fluctuation range lower than 0.58 Å. At the same time, we monitor the kinetic energy, potential energy and total energy of the system (Fig. 3). As seen from Fig. 3, three energies of the system are very stable during MD simulation. The above analyses show that the dynamics equilibrium of the system is reliable.

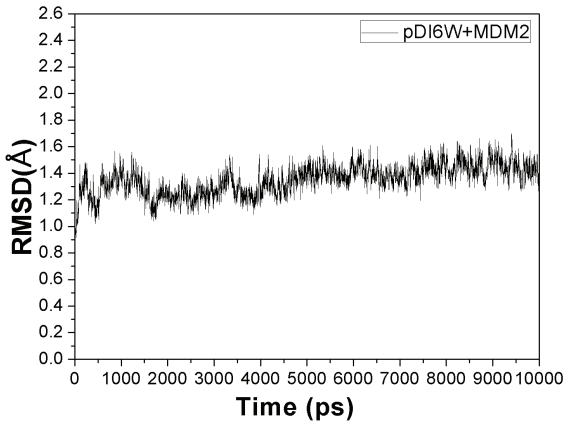

Figure 2: Root-Mean-Square Deviation of the backbone atoms on the pDI6W-MDM2 complex.

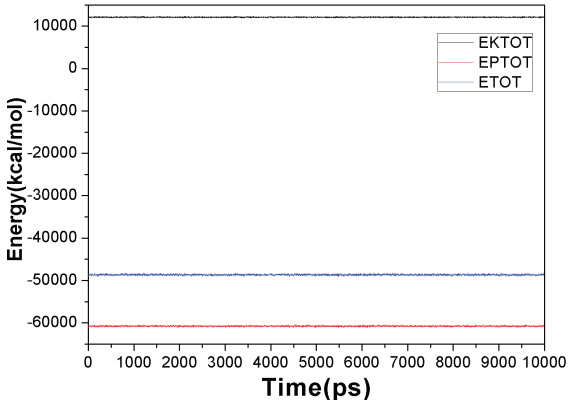

Figure 3: The energies of the pDI6W-MDM2 complex as function of time observed during MD simulation, EKTOT (up)EPTOT(down) and ETOT(middle).

3.2 Cross-correlation analysis

To understand the conformation change of MDM2 induced by the pDI6W binding, cross-correlation matrices of the fluctuations are calculated and plotted in Fig. 4. The extent of correlation or anticorrelation in the motion between specific residues is depicted in a color-coded manner. As shown in the Fig. 4, the presence of pDI6W results in the obvious anticorrelations within MDM2 (dark blue), but the correlations motion are not obvious.

According to Fig. 4, the subunit S3 moves relative to S2 and S4 in an anticorrelation manner. Some weak anticorrelations are observed between the subunit S2 and S4. Additionally, obvious anticorrelations also occur in the subunit S3. Except for the correlation motion in S1 and S2, the subunit S3 moves relative to S4 in the correlation mode.

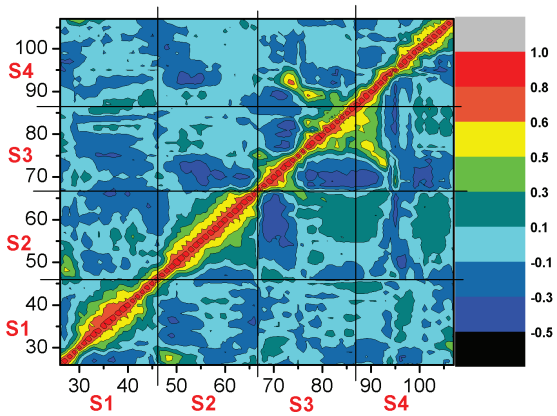

Figure 4: Cross-correlation matrices of the fluctuations of the coordination for $C\alpha$ atoms aruond their mean positions after the equilibrium of system.

3.3 The calculation of binding free energy

The binding free energies of inhibitors to proteins not only indicate their binding strength, but also reflect the main forces of their binding. Thus, the MM-PBSA method is applied

Table 1: Results calculated by MM-PBSA methoda[a].

Component	pDI6W-MDM2		MDM2		pDI6W		Delta	
E_{ele}	-2264.39	44.66	-1876.70	36.17	-252.49	12.02	-135.20	18.19
E_{vdw}	-407.57	16.34	-322.30	16.10	-19.52	4.63	-67.76	3.43
E_{int}	2199.34	29.62	1929.63	30.11	269.71	10.96	-0.00	0.00
E_{gas}	-472.63	44.31	-269.37	40.94	-2.29	15.24	-202.96	17.40
G_{surf}	34.13	0.59	32.51	0.60	9.43	0.22	-7.81	0.19
G_{pb}	-1262.33	35.94	-1150.88	29.35	-264.65	11.56	153.20	14.88
G_{sol}	-1228.20	35.72	-1118.37	29.17	-255.22	11.43	145.39	14.80
G_{pbele}	-3526.73	17.34	-3027.58	15.25	-517.14	4.87	17.99	4.99
G_{pbtot}	-1700.83	29.04	-1387.74	29.07	-257.52	10.71	-56.57	4.38
TS_{tra}	16.24	0.00	16.13	0.00	14.34	0.00	-14.23	0.00
TS_{rot}	16.15	0.00	16.02	0.01	12.95	0.00	-12.82	0.01
TS_{vib}	1279.01	2.94	1139.01	3.22	149.73	0.52	-9.74	2.48
TS_{tot}	1311.40	2.94	1171.16	3.23	177.02	0.52	-36.78	2.49
ΔG_{bind}								-19.79

[a] E_{ele} and E_{vdw} are electrostatic energy and van der Waals energy, respectively; E_{int} is internal energy; $E_{gas} = E_{ele}+E_{vdW}+E_{int}$; G_{pb} and G_{surf} are non-polar and polar solvation energies, respectively; solvation energy $G_{sol}=G_{pb}+G_{surf}$; $G_{pbele}=E_{ele}+G_{pb}$; $G_{pbtot}=E_{ele}+E_{vdW}+E_{int}+G_{pb}+G_{surf}$; TS_{tra}, TS_{rot} and TS_{vib} represent the contribution of entropy change to the free energy caused by the changes of the translational, rotational and vibrational of freedom; $TS_{tot}=TS_{tra}+TS_{rot}+TS_{vib}$; $\Delta G_{bind}=\Delta G_{pbtot}-T\Delta S$.

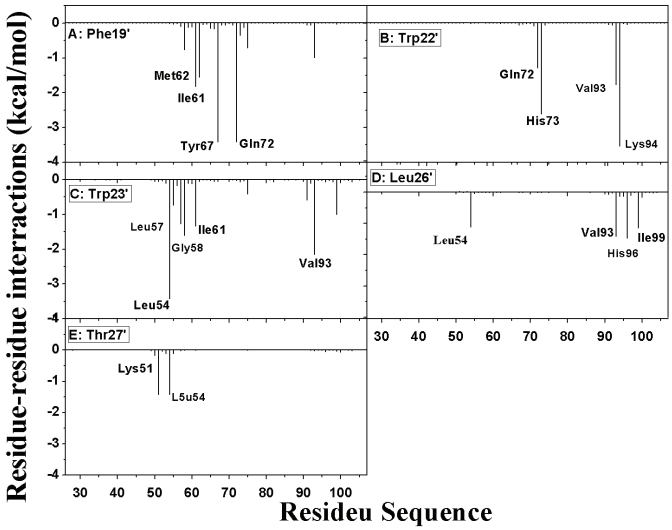

Figure 5: Residue-residue interaction spectrum between the inhibitor pDI6W and MDM2.

to calculate the binding free energy of pDI6W to MDM2, and the results are listed in Table 1.

According to 1, the binding free energy of pDI6W to MDM2 is -19.79 kcalmol-1, which shows that their binding is strong. The van der Waals energy (ΔG_{vdw}) between pDI6W and MDM2 is -67.76 kcal·mol^{-1}. This interaction provides a favorable contribution to the binding. The non-polar solvation energy (-7.81 kcal·mol^{-1}), which correspond to the burial of SASA upon binding, also provides the favorable contribution. Although the electrostatic terms (ΔG_{ele}) favor inhibitor binding, this favorable contribution is completely screened by the stronger unfavorable polar solvation energy (ΔG_{pb}). In the case of two favorable contributions, the van der Waals energy is almost nine times more than the non-polar solvation energy. Therefore, the van der Waals energy mostly drives the binding of pDI6W to MDM2. The above analyses agree basically with the results Jiang *et al.*[13] and Cheng *et al.*[21].

3.4 Analyses of structure-affinity relationship

To quantificationally probe the binding mode of pDI6W to MDM2 and clarify their structure-affinity relationship, we use the residue-based free energy decomposition method to calculate the interactions of pDI6W with separate residues of MDM2 (Fig. 5). Fig. 6 depicts the relative positions of key residues in the complex. Fig. 5 shows that five residues of pDI6W can produce strong interactions with MDM2. This result suggests that pDI6W can compete with p53 and efficiently inhibit the p53-MDM2 interaction.

According to Fig. 5A, the residue Phe19′ of pDI6W generates strong interactions with four residues of MDM2. These four residues are Ile61, Met62, Tyr67 and Gln72. The inter-

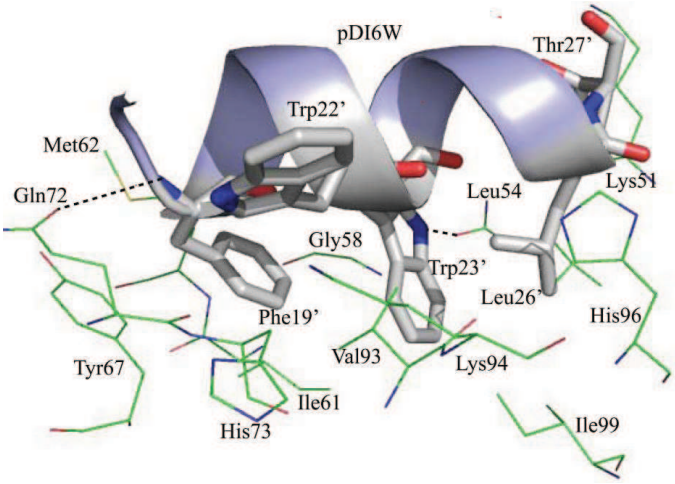

Figure 6: Relative geometries of the key residues in pDI6W-MDM2 complex and hydrogen bonds.

action energy of Phe19′ with Tyr67 is -3.42 kcal·mol^{-1}, which agrees structurally with the $\pi-\pi$ interaction between two phenyls of Phe19′ and Tyr67 (Fig. 6)[22]. As seen from Fig. 6 and Table 2, a hydrogen bond is formed between Phe19′ and Gln72, which contribute a interaction energy of -3.41 kcal·mol^{-1} to the inhibitor binding. The interaction energies of Phe19′ with Ile61 and Met62 are -1.82 and -1.55 kcal·mol^{-1}, respectively. These two interaction energies mainly come from the CH-π interactions of CH groups from Ile61 and Met62 with the phenyl of Phe19′. Therefore, Ile61, Met62, Tyr67 and Gln72 form the first hydrophobic binding pocket of pDI6W.

As shown in Fig. 5C, the residue Trp23′ of pDI6W produces strong interactions with five residues (Leu54, Leu57, Gly58, Ile61 and Val93) of MDM2. The interaction energy of Trp23′ with Leu54 is -3.43 kcal·mol^{-1}. This energy mostly comes from two contributions: (1) the CH-π interactions of the alkyl in Leu54 with the indole of Trp23′, (2) a hydrogen bond formed between the nitrogen atom in the indole of Trp23′ and the backbone carbonyl oxygen O of Leu54 (Table 2 and Fig. 6). According to Fig. 6, structurally, the CH groups of four residues Leu57, Gly58, Ile61 and Val93 from MDM2 are near the indole of Trp23′, they respectively produce the CH-π interactions of -1.27, -1.61, -1.34 and -2.16

Table 2: The hydrogen bonds of the key residues.

Donor[a]	Acceptor[b]	Distance[c] / Å	Angle[d] /(○)	Freq.[e] /%
Phe19-N-H	Gln72-OE1	3.102	148.83	45.12
Trp23-NE1-HE1	Leu54-OE1	2.889	150.97	91.34

[a] The donor of hydrogen bond;
[b] The Acceptor of hydrogen bond;
[c] The distance between the acceptor and donor atom;
[d] The angle of the the acceptor...H-donor atom.

kcal·mol^{-1} with Trp23′. Therefore, five residues Leu54, Leu57, Gly58, Ile61 and Val93 shape the second hydrophobic binding pocket of pDI6W.

According to Fig. 5D, four residues Leu54, Val93, His96 and Ile99 of MDM2 produce the interactions stronger than -1.1 kcal·mol^{-1} with the residue Leu26′ of pDI6W. The interaction energies of Leu26′ with Leu54, Val93 and His96 are -1.11, -1.41 and -1.14 kcal·mol^{-1}, respectively, which agree structurally with the CH-CH interactions of the alkyls from Leu54Val93 and His96 with the alkyl of Leu26′ (Fig. 6). The interaction energy of Leu26′ with His96 is -1.47 kcal·mol^{-1}, which mainly comes from the CH-π interactions between the alkyl of Leu26′ and the ring of His96. Thus, the residues Leu54, Val93, His96 and Ile99 build the third hydrophobic binding pocket of pDI6W.

As seen from Fig. 5B and Fig. 5E, two additional residues (Trp22′ and Thr27′) also provide important contributions to the inhibitor binding. The interaction energies of Trp22′ with Gln72, His73, Val93 and Lys94 are -1.29, -2.61, -1.77 and -3.54 kcal·mol^{-1}, respectively, these interaction energies mostly root in the CH-π interactions of the indole in Trp22 with the alkyls of Gln72, His73, Val93 and Lys94 (Fig. 6). According to Fig. 5E, the residue Thr27′ of pDI6W respectively generates the interactions of -1.42 and -1.43 kcal·mol^{-1} with Lys51 and Leu54, which mainly are contributed by the CH-CH interactions of the alkyls of Lys51 and Leu54 with the alkyl of Thr27′. The residues Trp22′ and Thr27′ imitate the interactions of Leu22′ and Pro27′ in p53 with MDM2. This imitation results in the efficient inhibition effect on the p53-MDM2 interactions. The above analyses agree basically with the quantum mechanics studies of Ding *et al.*[23] and molecular mechanics studies of Cheng *et al.*[21] and Liu *et al.*[12]. To sum up, the CH-CHCH-π and $\pi-\pi$ interactions drive the binding of pDI6W to MDM2.

4 Conclusions

10 ns MD simulation is performed on the pDI6W-MDM2 complex to study the conformation change of MDM2 induced by the inhibitor binding. The results of the cross-correlation matrix suggest that the presence of pDI6W mostly induce the anticorrelation motion in MDM2. The calculation of the binding free energy by using the MM-PBSA method proves that the van der Waals energy drives the binding of pDI6W to MDM2. The residue-residue interactions calculated by the residue-based free energy decomposition method show that Phe19′, Trp22′, Trp23′, Leu26′ and Thr27′ of pDI6W produce strong interactions with MDM2. We expect that this study can contribute significant helps to the designs of anticancer drugs.

Acknowledgments We acknowledge financial support from the National Nature Science Foundation (Grant No. 11104164), Dr. Start-up Foundation for Shandong Jiaotong University and Science Foundation of School for Shandong Jiaotong University.

References

[1] Y. Haupt, R. Maya, A. Kazaz, and M. Oren, Nature 387 (1997) 296.
[2] T. L. Joseph, A. Madhumalar, C. J. Brown, D. P. Lane, and C. Verma, Cell 9 (2010) 1167.
[3] H. F. Chen and R. Luo, J. Am. Chem. Soc. 129 (2007) 2930.
[4] L. T. Vassilev, B. T. Vu, B. Graves, D. Carvajal, F. Podlaski, Z. Filipovic, N. Kong, U. Kammlott, C. Lukacs, and C. Klein, Science 303 (2004) 844.
[5] G. M. Popowicz, A. Czarna, and S. Wolf, Cell 9 (2010) 1104.
[6] M. Pazgier, M. Liu, G. Zou, W. Yuan, C. Li, J. Li, J. Monbo, D. Zella, and S. G. Tarasov, Proc. Natl. Acad. Sci. 106 (2009) 4665.
[7] K. Ding, Y. Lu, Z. Nikolovska-Coleska, G. Wang, S. Qiu, S. Shangary, W. Gao, D. Qin, J. Stuckey, and K. Krajewski, J. Med. Chem. 49 (2006) 3432.
[8] J. Phan, Z. Li, A. Kasprzak, B. Li, S. Sebti, W. Guida, E. Schönbrunn, and J. Chen, J. Biol. Chem. 285 (2010) 2174.
[9] J. Chen, S. Zhang, X. Liu, and Q. Zhang, J. Mol. Model. 16 (2010) 459.
[10] J. Chen, J. Wang, B. Xu, W. Zhu, and G. Li, J. Mol. Graph. Model. (2011) 46.
[11] E. L. Wu, K. L. Han, and J. Z. H. Zhang, Chem. Eur. J. 14 (2008) 8704.
[12] S. Y. Lu, Y. J. Jiang, J. W. Zou, and T. X. Wu, J. Mol. Graph. Mod. 30 (2011) 167.
[13] Y. J. Jiang, M. Zeng, X. B. Zhou, J. W. Zou, and Q. S. Yu, Acta Chim. Sin. 62 (2004) 1751.
[14] G. D. Hu, S. L. Zhang, X. G. Liu, and Q. G. Zhang, J. At. Mol. Phys. 27 (2010) 333.
[15] E. L. Wu, Y. Mei, K. L. Han,and J. Z. H. Zhang, Biophys. J. 92 (2007) 4244.
[16] C. H. Yi, J. Z. Chen, T. Zhu, and Q. G. Zhang, J. At. Mol. Phys. 28 (2011) 11.
[17] G. Hu, D. Wang, X. Liu, and Q. Zhang, J. Comp. Aid. Mol. Des. 24 (2010) 687.
[18] J. P. Hu, T. G. Sun, W. Z. Chen, and C. X. Wang, Acta Chim. Sin. 64 (2006) 2079.
[19] D. A. Case, T. A. Darden, T. E. Cheatham III, C. L. Simmerling, J. Wang, R. E. Duke, R. Luo, R. C. Walker, W. Zhang, K. M. Merz, S. Roberts, S. Hayik, A. Roitberg, G. Seabra, J. Swails, A. W. G?tz, I. Kolossvry, K. F. Wong, F. Paesani, J. Vanicek, R. M. Wolf, J. Liu, X. Wu, S. R. Brozell, T. Steinbrecher, H. Gohlke, Q. Cai, X. Ye, J. Wang, M.-J. Hsieh, G. Cui, D. R. Roe, D. H. Mathews, M. G. Seetin, R. Salomon-Ferrer, C. Sagui, V. Babin, T. Luchko, S. Gusarov, A. Kovalenko, and P. A. Kollman, AMBER 12 (University of California, San Francisco, 2012).
[20] T. G. Coleman, H. C. Mesick, and R. L. Darby, Ann. Biomed. Eng. 5 (1977) 322.
[21] W. Y. Cheng, Z. Q. Liang, Q. G. Zhang, C. H. Yi, W. Wang, and K. Y. Wang, J. At. Mol. Phys. 29 (2012) 393.
[22] Y. Ding, Y. Mei, J. Z. H. Zhang, and F. M. Tao, J. Comput. Chem. 29 (2008) 275.
[23] Y. Ding, Y. Mei, and J. Z. H. Zhang, J. Phys. Chem. B 112 (2008) 11396.